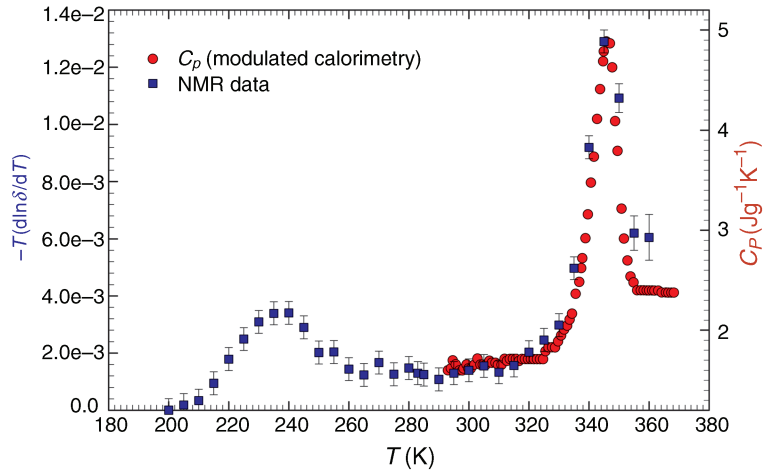

Figure 11.1. A comparison between the conformational heat capacity obtained from NMR [15] and calorimetric C_P data in the water–lysozyme system [14].

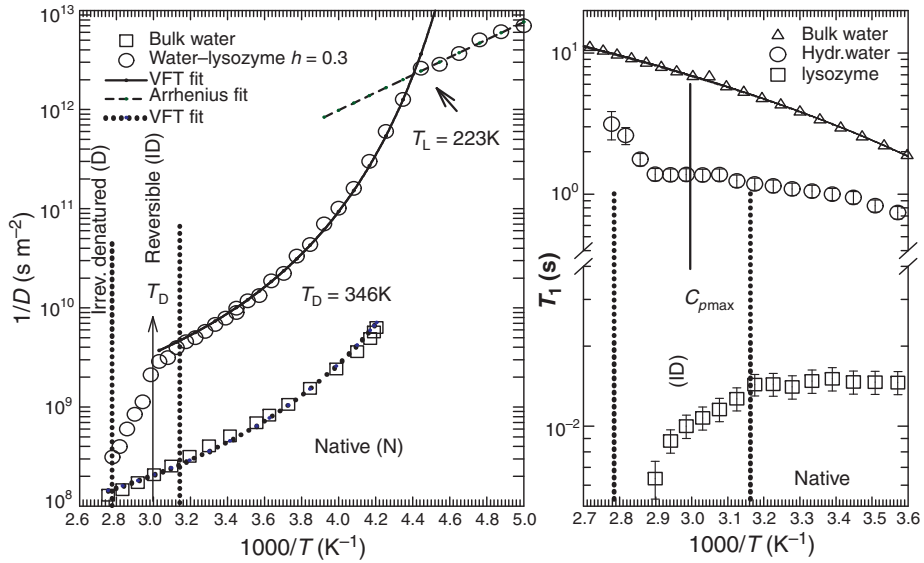

Figure 11.3. (**a**) The inverse of the NMR self diffusion coefficient $1/D$ versus $1/T$ (squares the bulk water and circles the protein hydration one). The, $1/D$ behavior identifies two crossovers: one at the FSC temperature T_{L} (223K) and one at a higher temperature (T_{D}) in the region of the protein denaturation. (**b**) The thermal evolution of the longitudinal NMR relaxation time T_1 [19].

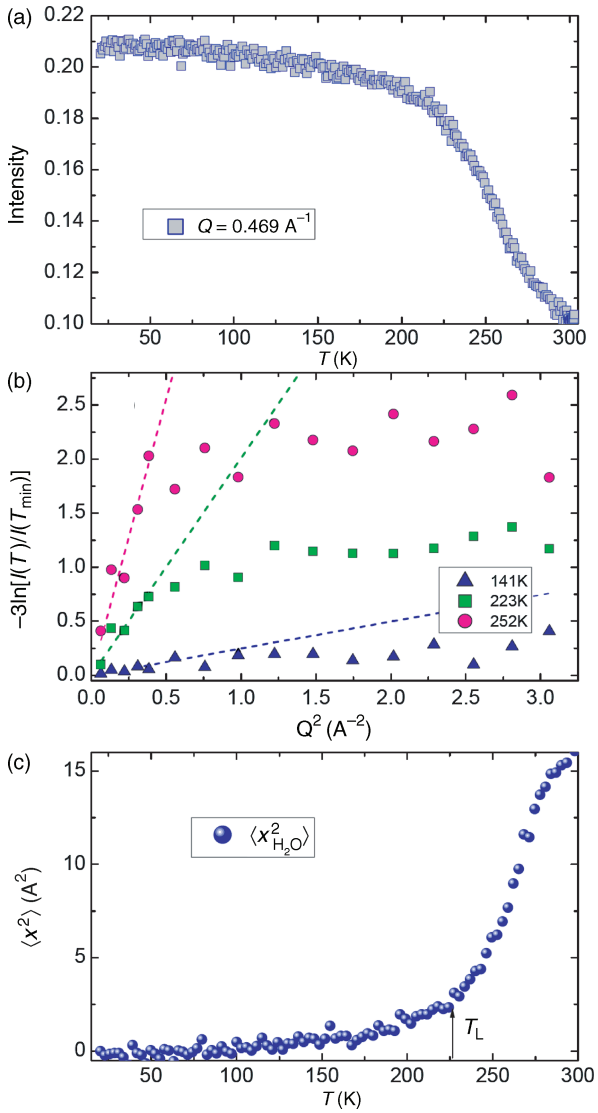

Figure 11.4. Data analysis method used to obtain $\langle X^2_{H_2O} \rangle$ of RNA hydration water. (**a**) The so-called elastic scan. (**b**) The logarithm of intensity versus Q^2 at three temperatures. (**c**) The extracted MSD of the hydration water as a function of temperature.

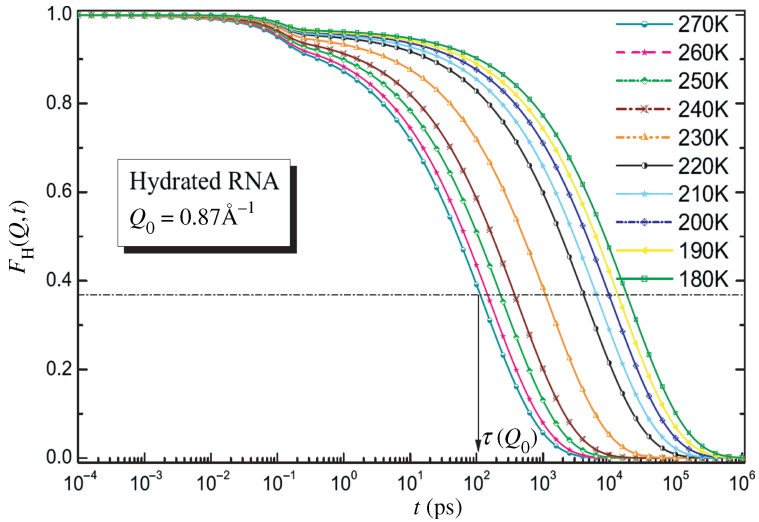

Figure 11.5. The $F_H(Q, t)$ extracted from the quasi-elastic neutron spectra by using the RCM at Q_0 in RNA hydration water at different T.

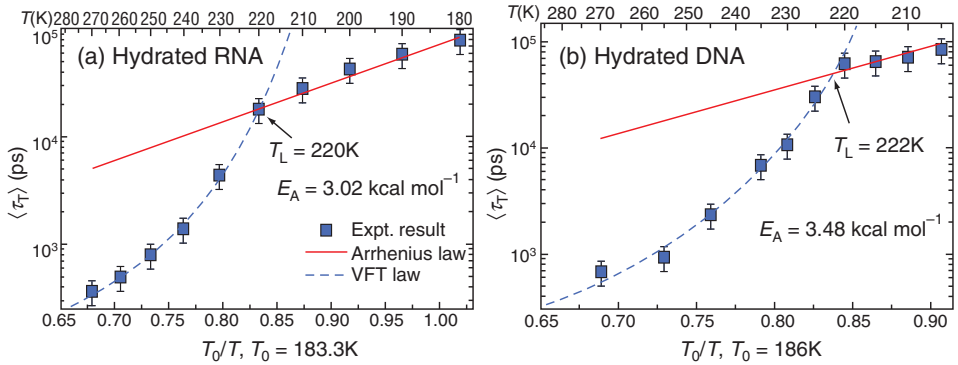

Figure 11.6. (**a**) The RCM $\langle \tau_T \rangle$ versus T. A dynamic crossover is observed at $T_L = 220$K. The dashed line is the VFT data fit, and the solid line the Arrhenius law. (**b**) A similar analysis for a hydrated DNA where $T_L = 222$K [26].

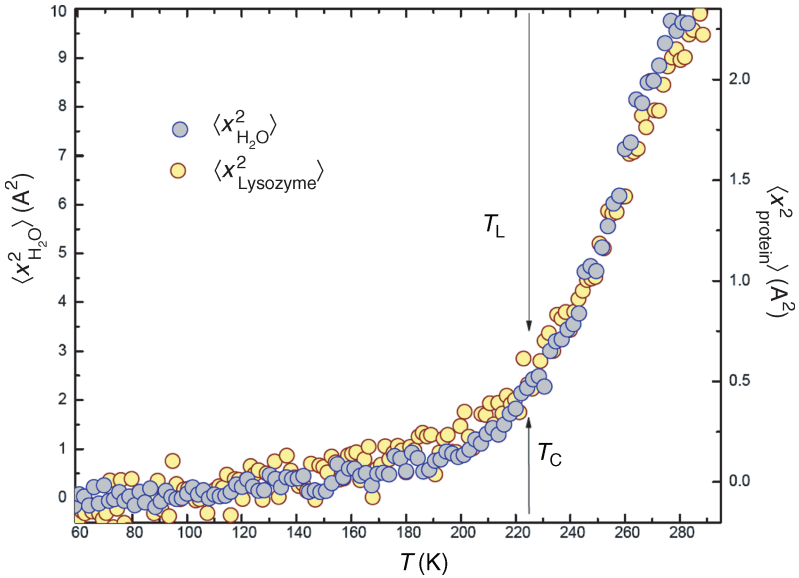

Figure 11.7. The MSDs measured for the protein (left) and its hydration water (right). The protein MSD is taken from the D_2O hydrated sample.

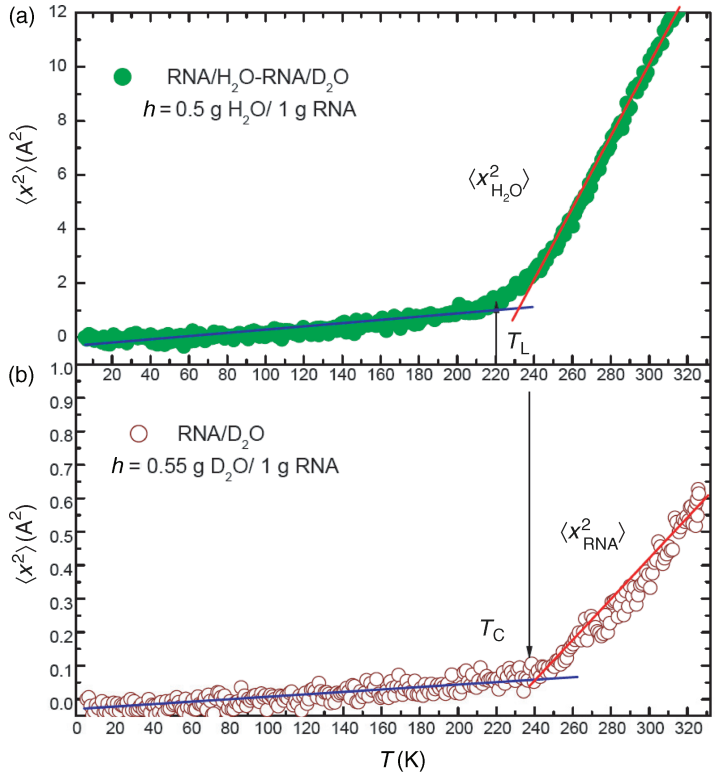

Figure 11.8. The slope of the MSD versus T curve used as a measure of biomaterial softness. Above the crossover temperature, RNA becomes 15 times softer than its glassy state and hydration water becomes 20 times softer [26].

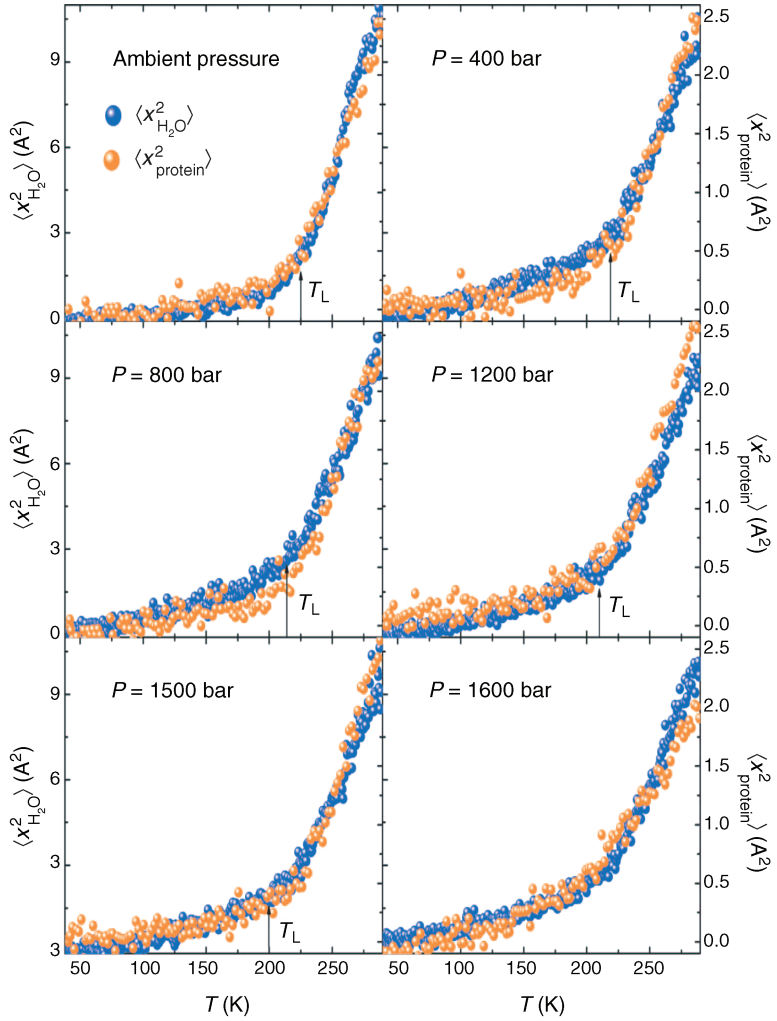

Figure 11.9. Reduced plot of pressure dependence of MSD of protein and its hydration water [29].

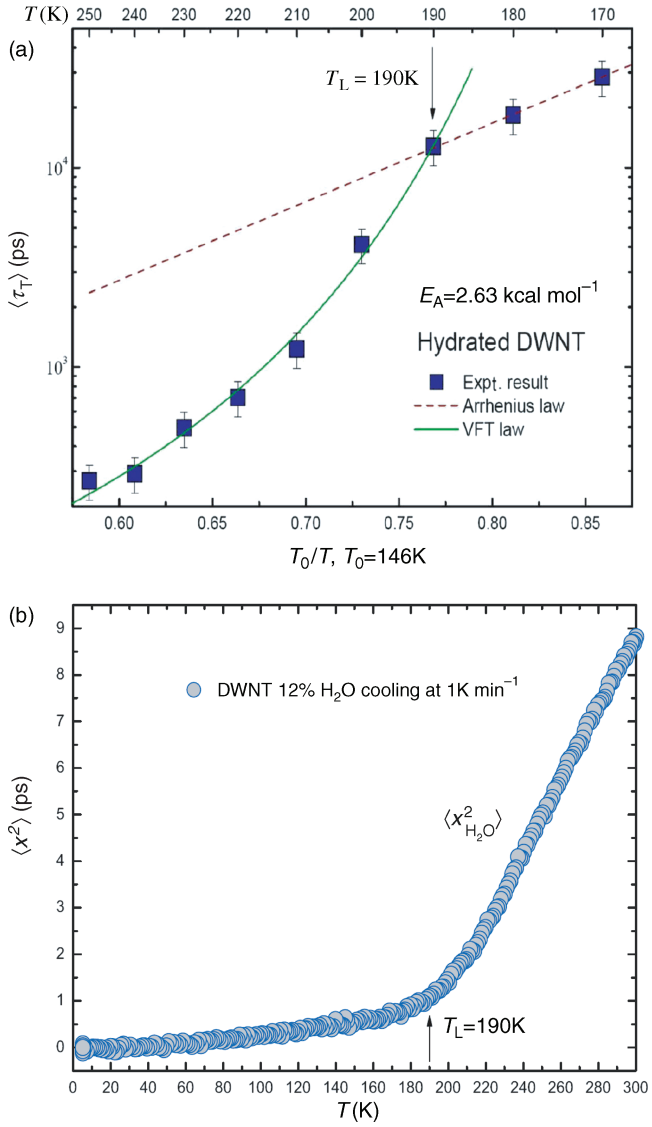

Figure 11.10. (**a**) The $\langle \tau_T \rangle$ versus $1/T$ of water in hydrophobic nanotubes (DWNT). The solid and dashed lines represent the VFT and the Arrhenius law fits, respectively. (**b**) The MSD versus T averaged over all the extracted hydrogen atoms, $\langle X^2 \rangle$ [31].

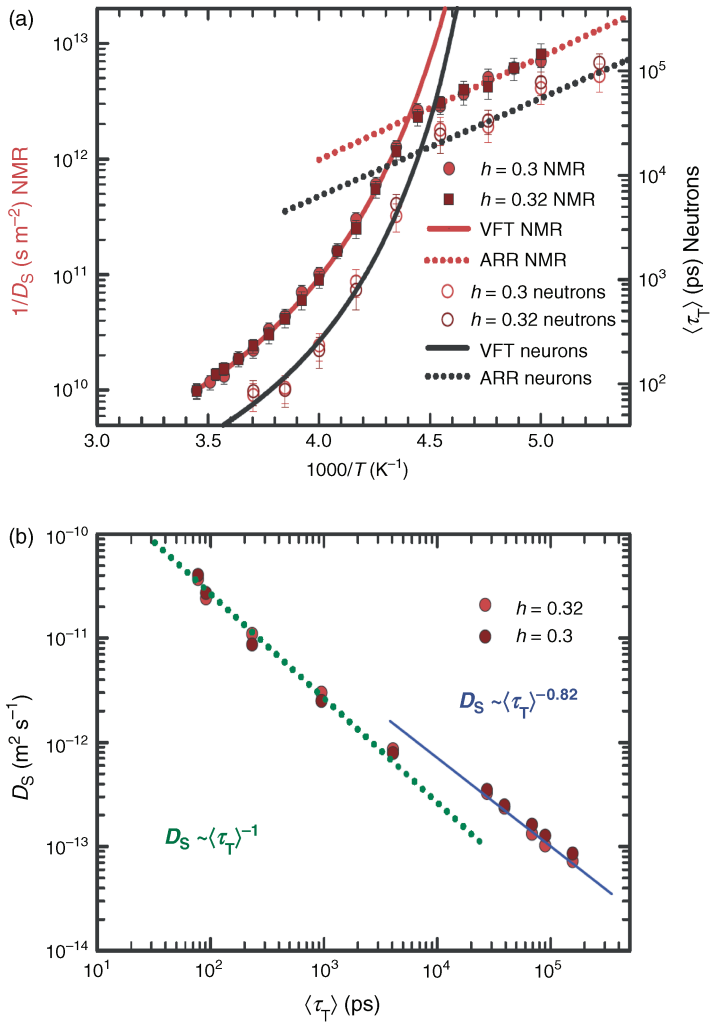

Figure 11.11. (**a**) The NMR $1/D$ (left) and the QENS relaxation time $\langle\tau_T\rangle$ (right), versus $1/T$. The FSC are at $T_{L,NMR} = 226 \pm 2$K and $T_{L,QENS} = 225 \pm 2$K. (**b**) The scaled SER, $\log D_S$ versus $\log\langle\tau_T\rangle$. Two scaling behaviors above and below T_L are observed: in the super-Arrhenius region $\xi \approx 1$, and in the Arrhenius region $\xi \approx 0.82$.

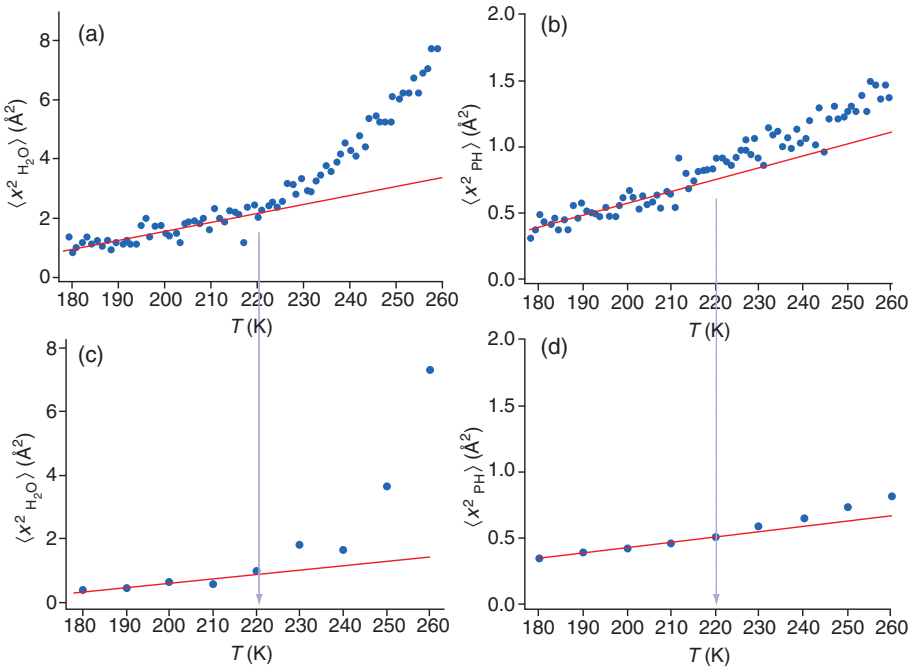

Figure 11.13. The hydrogen MSD, $\langle X^2 \rangle$, measured by elastic neutron scattering, that is, (**a**) protein hydration water and (**b**) protein hydrogen atoms, and by simulations, that is, (**c**) protein hydration water and (**d**) protein hydrogen atoms [51].

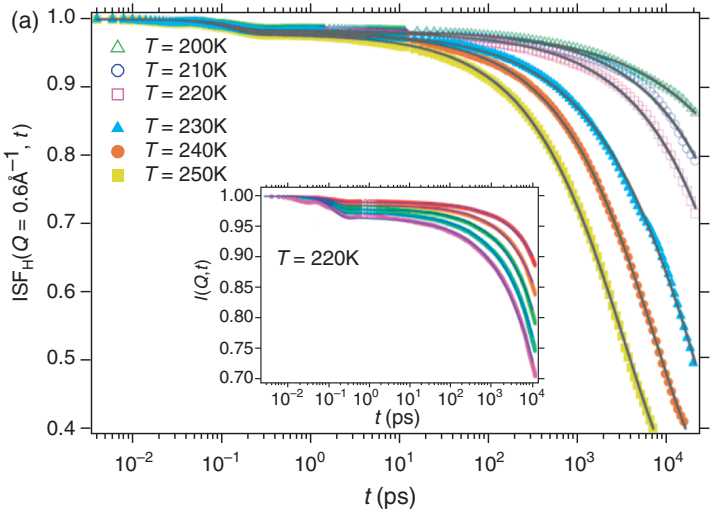

Figure 11.14. The Water proton incoherent self-ISF calculated at six different T. The ISF at five different Q values (from top to bottom, 0.4, 0.5, 0.6, 0.7, and 0.8 Å^{-1}), inset. The solid curves are fit to the RCM [51].

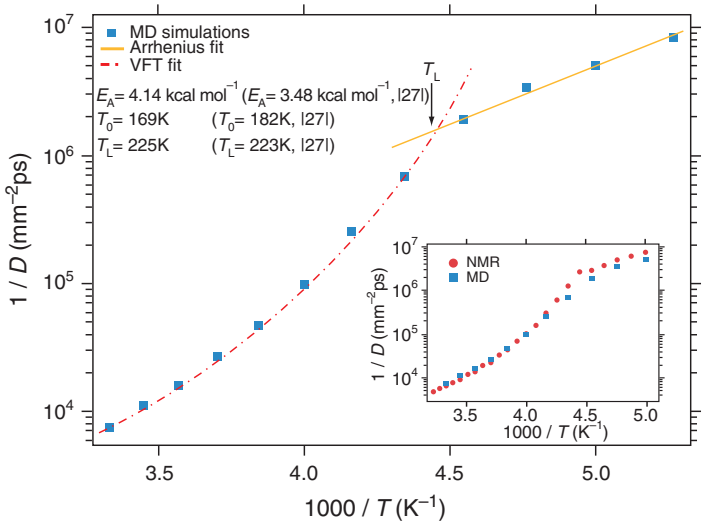

Figure 11.15. T-dependence of the inverse diffusion constant, $1/D$, from MD simulations. Comparison between MD simulations and NMR data [19] (inset) [51].

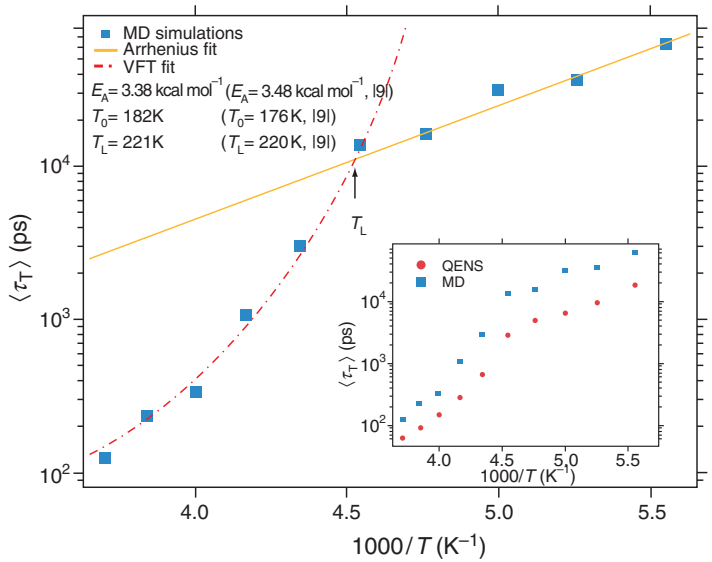

Figure 11.16. T-dependence of the average translational relaxation time, $\langle \tau_T \rangle$, from MD simulation [51]. Comparison between MD simulation and QENS data [17] (inset).

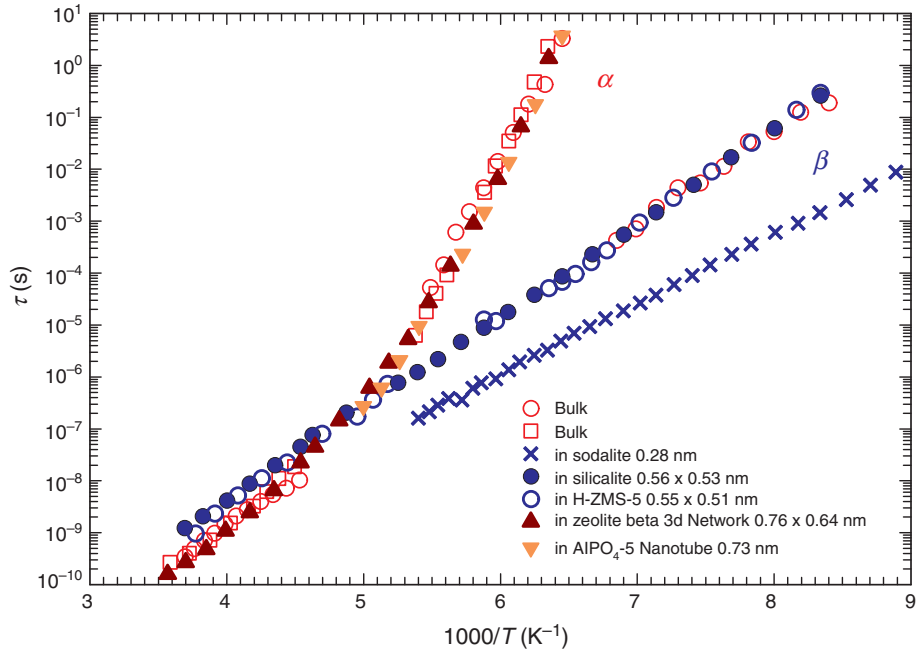

Figure 11.17. The ethylene glycol (EG), bulk [53,54] and confined in different geometries, dielectric relaxation times (τ) as a function of T.

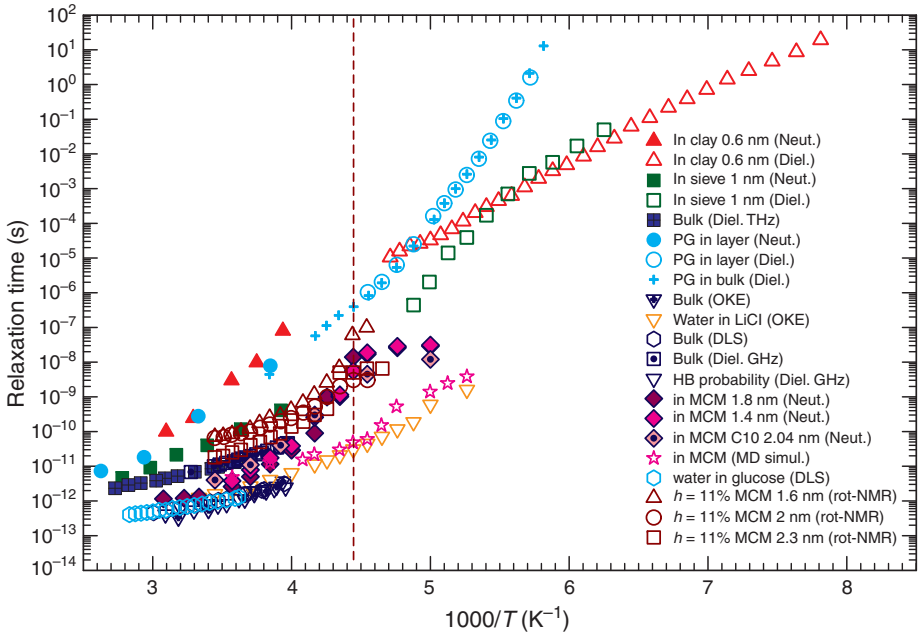

Figure 11.18. Relaxation times versus $1000/T$, measured for water in bulk [55–58] and in confining geometries [59–68]. Propylene glycol data are also reported [69,70]. Dashed line indicates T_{L}.

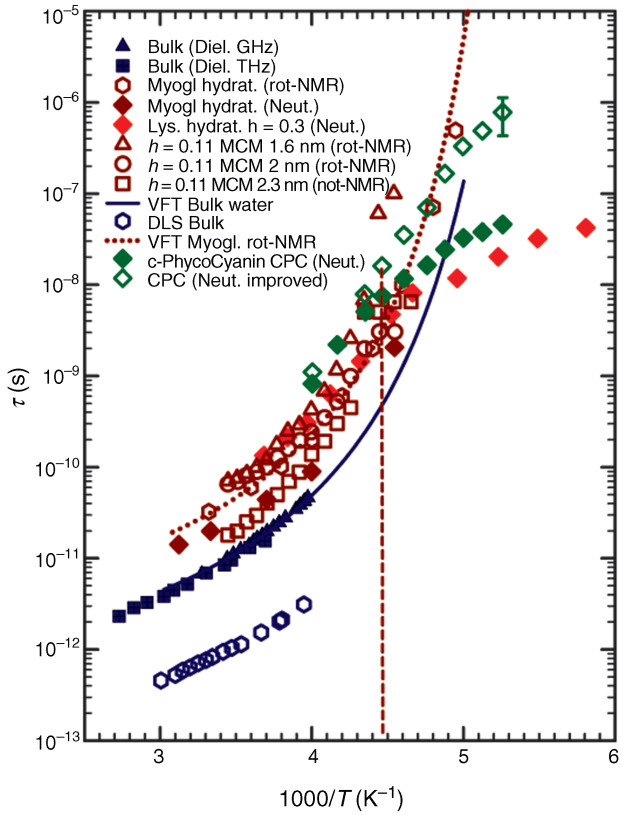

Figure 11.19. The relaxation times (τ vs. $1000/T$) of different protein hydration water, surface water of MCM-41, and bulk water. The dashed line indicates T_{L}.

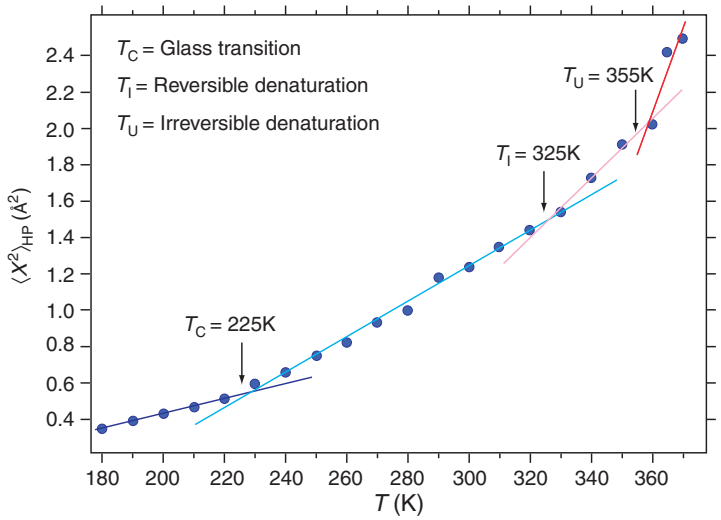

Figure 11.21. $\langle X^2 \rangle_{\mathrm{HP}}$ as a function of T for protein hydrogen atoms calculated from MD simulations [74].

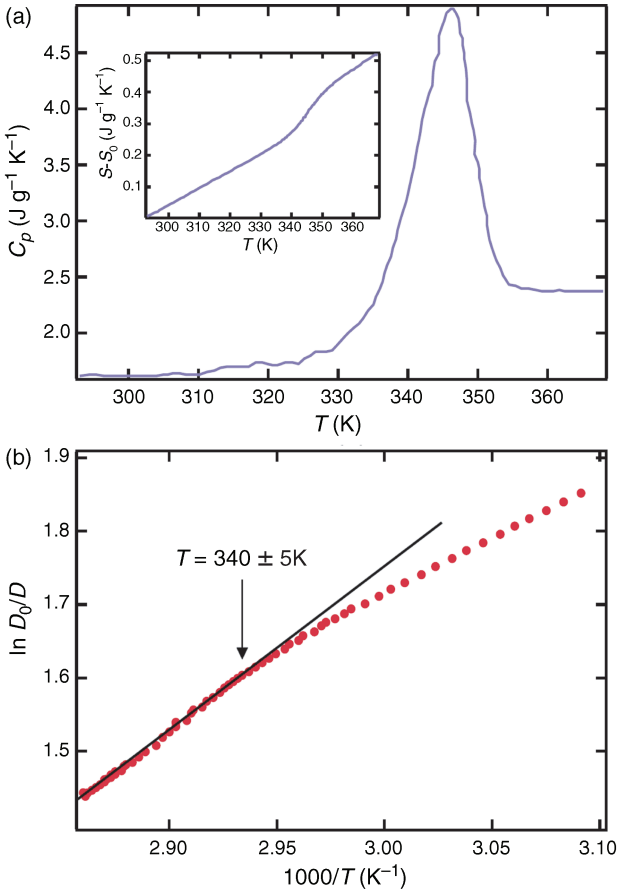

Figure 11.22. (**a**) Experimental C_P of a water–lysozyme solution [14] Inset: $S(T)$ versus T calculated from integration of the experimental C_P. (**b**) Arrhenius plot of D_0/D versus $1000/T$ obtained according to the Adam–Gibbs equation [74].

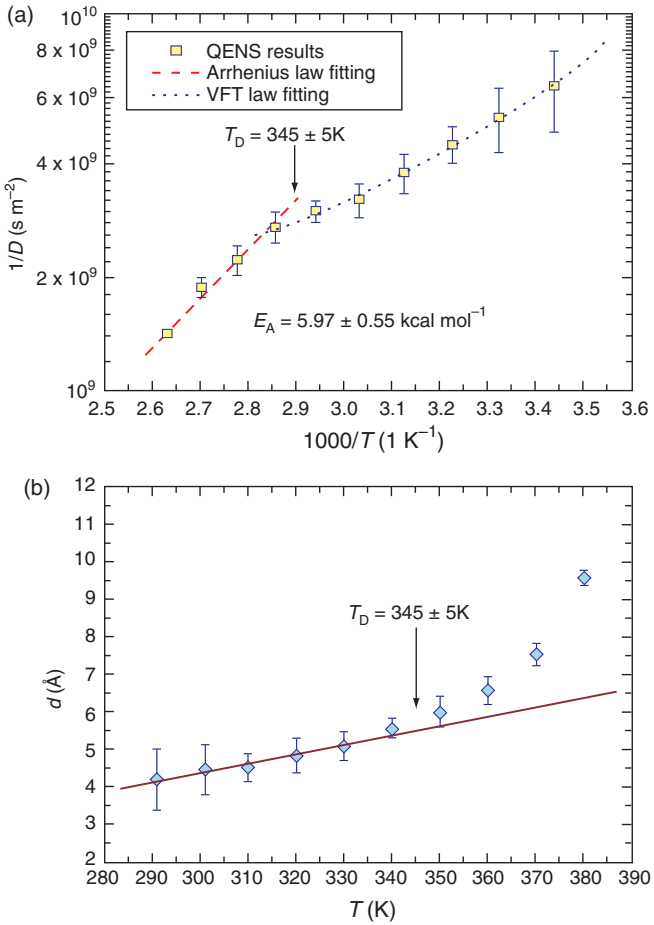

Figure 11.23. (**a**) The plot of experimentally extracted $1/D$ versus $1000/T$ of the protein hydration water shows the dynamic crossover as T is raised through $T_D = 345 \pm 5$K. (**b**) Plot of experimentally extracted average migration distance d of the hydration water [74].

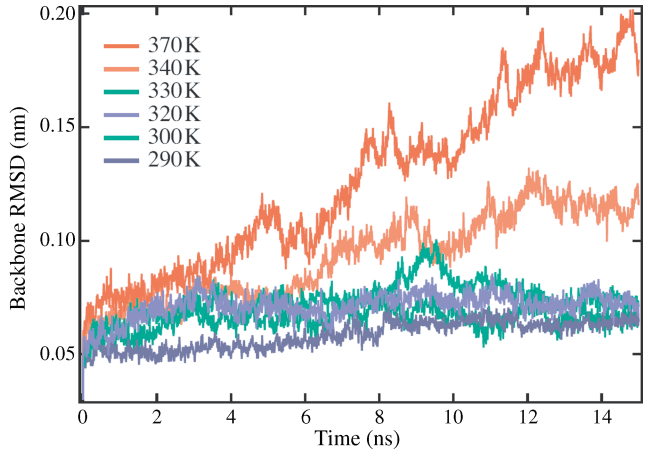

Figure 11.24. The backbone RMSD as a function of t at different T. No remarkable change is detected until 340K when the protein increases its flexibility [74].

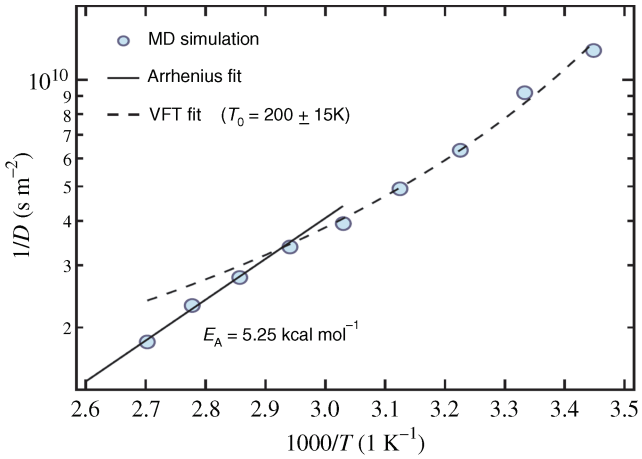

Figure 11.25. Arrhenius plot of the $1/D$ for lysozyme hydration water, calculated from MD simulations. The curve shows an high-T dynamic crossover similar to the one observed by QENS (Fig. 24) [74].

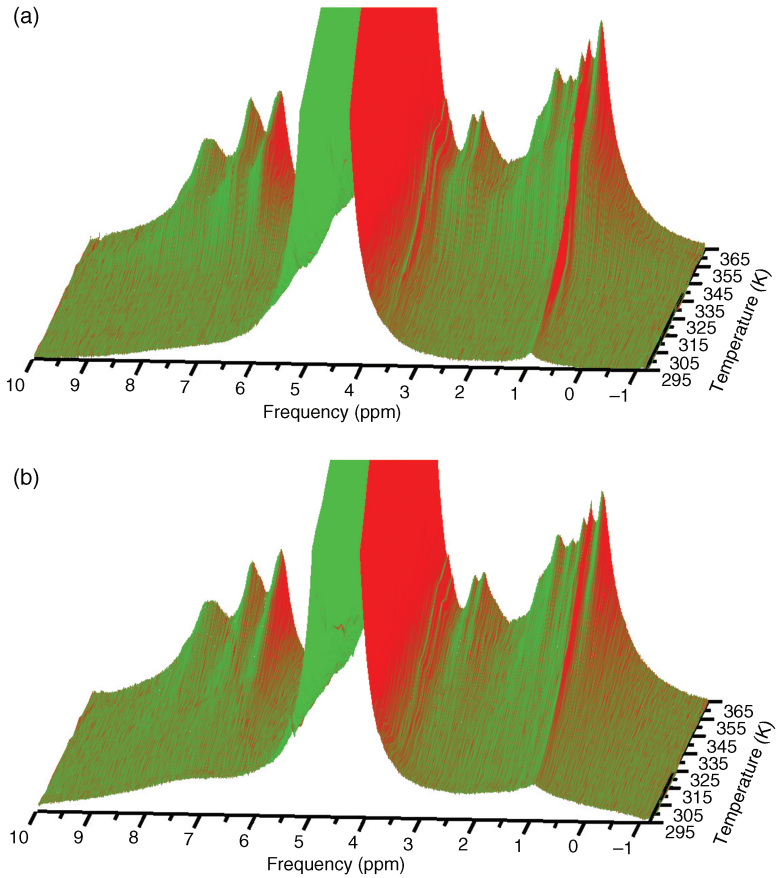

Figure 11.26. The ^{1}H NMR spectra (obtained from the FID, cycle A) of hydrated lysozyme ($h = 0.3$) upon the warming (**a**) and cooling (**b**) phases.

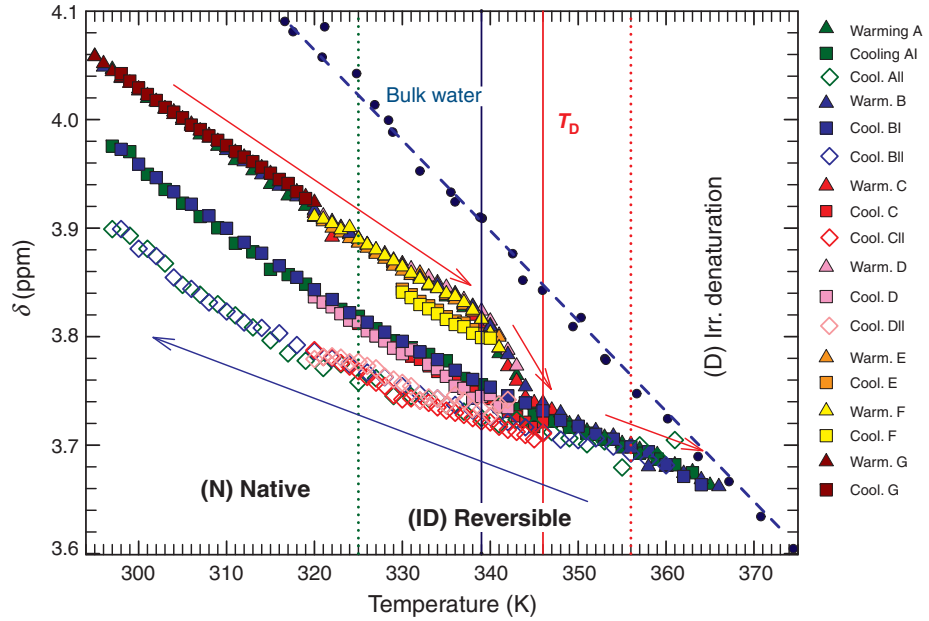

Figure 11.27. The evolution of the ^{1}H NMR chemical shift $\delta(T)$ in several thermal cycles of the lysozyme water. The pure bulk water chemical shift are also reported.

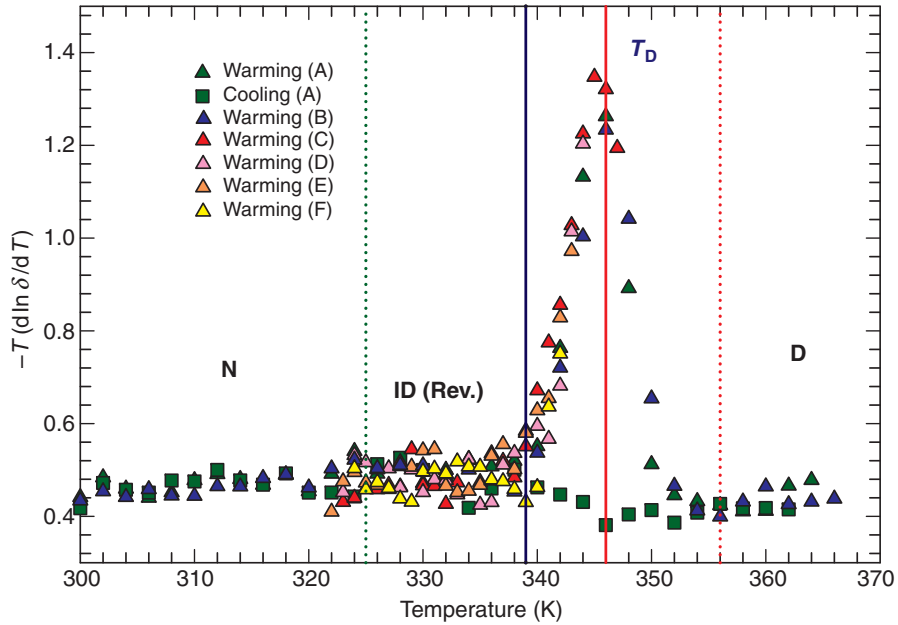

Figure 11.28. The configurational specific heat for all the cycles. It is worth noticing that the value of the obtained maximum is, within the experimental error, the same of that measured by high-resolution calorimeters.